

Relativistic energy density functional description of shape transitions in superheavy nucleiV. Prassa,^{1,2,3} T. Nikšić,¹ G. A. Lalazissis,² and D. Vretenar¹¹*Physics Department, Faculty of science, University of Zagreb, 10000 Zagreb, Croatia*²*Department of Theoretical Physics, Aristotle University of Thessaloniki, Thessaloniki Gr-54124, Greece*³*Department of Physics, P.O. Box 35 (YFL), FI-40014 University of Jyväskylä, Finland*

(Received 7 May 2012; revised manuscript received 9 August 2012; published 30 August 2012)

Relativistic energy density functionals (REDF) provide a complete and accurate global description of nuclear structure phenomena. A modern semiempirical functional, adjusted to the nuclear matter equation of state and to empirical masses of deformed nuclei, is applied to studies of shapes of superheavy nuclei. The theoretical framework is tested in a comparison of calculated masses, quadrupole deformations, and potential energy barriers to available data on actinide isotopes. Self-consistent mean-field calculations predict a variety of spherical, axial, and triaxial shapes of long-lived superheavy nuclei, and their α -decay energies and half-lives are compared to data. A microscopic, REDF-based, quadrupole collective Hamiltonian model is used to study the effect of explicit treatment of collective correlations in the calculation of Q_α values and half-lives.

DOI: [10.1103/PhysRevC.86.024317](https://doi.org/10.1103/PhysRevC.86.024317)

PACS number(s): 21.60.Jz, 21.10.Dr, 24.75.+i, 27.90.+b

I. INTRODUCTION

For many years theoretical studies of superheavy nuclei (SHN) were mostly based on the traditional macroscopic-microscopic approach [1–5], but since the late 1990s the framework of self-consistent mean-field models, based on realistic effective internucleon interactions or energy density functionals, has systematically been applied to the structure of SHN [5–23]. Binding energies, deformations, α -decay energies and half-lives, fission barriers and spontaneous-fission half-lives, fission isomers, and single-nucleon shell structure of SHN have successfully been described using self-consistent mean-field (SCMF) models based on the Gogny effective interaction, the Skyrme energy functional, and relativistic meson-exchange effective Lagrangians.

The advantages of using SCMF models include the intuitive interpretation of results in terms of single-particle states and intrinsic shapes, calculations performed in the full-model space of occupied states, and the universality that enables their applications to all nuclei throughout the periodic chart. The latter feature is especially important for extrapolations to regions of exotic, short-lived nuclei far from stability for which few, if any, data are available. In addition, the SCMF approach can be extended beyond the static mean-field level to explicitly include collective correlations and, thus, perform detailed calculations of excitation spectra and transition rates.

During the past decade, important experimental results on the mass limit of the nuclear chart have been obtained using compound nucleus reactions between the ^{48}Ca beam and actinide targets. A number of isotopes of new elements with the atomic number $Z = 113$ – 118 have been discovered, and new isotopes of $Z = 110$ and 112 [24–31]. The decay energies and the resulting half-lives provide evidence of a significant increase of stability with increasing neutron number in this region of SHN. Theoretical studies predict that SHN in this region should display rapid shape transitions, from prolate, through spherical, to oblate-deformed ground states [5,6,10,13,17,32]. These nuclei, therefore, present an ideal testing ground for structure models attempting to predict

the location of an “island of stability” for SHN around $N = 184$.

In this work we apply the framework of relativistic energy density functionals (REDF) to an illustrative study of shape transitions and shape coexistence in SHN with $Z = 110$ – 120 . There are several advantages in using functionals with manifest covariance and, in the context of this study, the most important is the natural inclusion of the nucleon spin degree of freedom and the resulting nuclear spin-orbit potential, which emerges automatically with the empirical strength. Our aim is to test the recently introduced functional DD-PC1 [33] in self-consistent relativistic Hartree-Bogoliubov (RHB) calculations of energy surfaces (axial, triaxial, octupole), α -decay energies, and half-lives of SHN, in comparison to available data and previous theoretical studies. Section II introduces the general framework of REDFs and, in particular, the functional DD-PC1 that will be used in illustrative calculations throughout this work. The functional is tested in calculations of binding energies, ground-state quadrupole deformations, fission barriers, fission isomers, and Q_α values for even-even actinide nuclei. In Sec. III, we apply the RHB framework based on the functional DD-PC1 and a separable pairing interaction in a description of triaxially deformed shapes and shape transitions of even-even superheavy nuclei. A microscopic, REDF-based, quadrupole collective Hamiltonian model is used to study the effect of explicit treatment of collective correlations. Q_α values and half-lives for two chains of odd-even and odd-odd superheavy systems are computed using a simple blocking approximation in axially symmetric self-consistent RHB calculations. Section IV summarizes the results and presents an outlook for future studies.

II. THE RELATIVISTIC ENERGY DENSITY FUNCTIONAL DD-PC1

Relativistic energy density functionals (REDF) provide an accurate, reliable, and consistent description of nuclear structure phenomena. Semiempirical functionals, adjusted to

a microscopic nuclear matter equation of state and to bulk properties of finite nuclei, are applied to studies of arbitrarily heavy nuclei, exotic nuclei far from stability, and even systems at the nucleon drip-lines. REDF-based structure models have been developed that go beyond the mean-field approximation and include collective correlations related to restoration of broken symmetries and to fluctuations of collective variables.

Although it originates in the effective interaction between nucleons, a generic density functional is not necessarily related to any given nucleon-nucleon potential and, in fact, some of the most successful modern functionals are entirely empirical. Until recently the standard procedure of fine-tuning global nuclear density functionals was to perform a least-squares adjustment of a small set of free parameters simultaneously to empirical properties of symmetric and asymmetric nuclear matter and to selected ground-state data of about ten spherical closed-shell nuclei. A new generation of semimicroscopic and fully microscopic functionals is currently being developed that will, on the one hand, establish a link with the underlying theory of strong interactions and, on the other hand, provide accurate predictions for a wealth of new data on short-lived nuclei far from stability. To obtain unique parametrizations, these functionals will have to be adjusted to a larger data set of ground-state properties, including both spherical and deformed nuclei [34,35].

For a relativistic nuclear energy density functional the basic building blocks are densities and currents bilinear in the Dirac spinor field ψ of the nucleon: $\bar{\psi}\mathcal{O}_\tau\Gamma\psi$, $\mathcal{O}_\tau \in \{1, \tau_i\}$, $\Gamma \in \{1, \gamma_\mu, \gamma_5, \gamma_5\gamma_\mu, \sigma_{\mu\nu}\}$. τ_i are the isospin Pauli matrices and Γ generically denotes the Dirac matrices. The isoscalar and isovector four-currents and scalar density are defined as expectation values of the corresponding operators in the nuclear ground state. The nuclear ground state is determined by the self-consistent solution of relativistic Kohn-Sham single-nucleon equations. To derive those equations it is useful to construct an interaction Lagrangian with four-fermion (contact) interaction terms in the various isospace-space channels: isoscalar-scalar $(\bar{\psi}\psi)^2$, isoscalar-vector $(\bar{\psi}\gamma_\mu\psi)(\bar{\psi}\gamma^\mu\psi)$, isovector-scalar $(\bar{\psi}\vec{\tau}\psi) \cdot (\bar{\psi}\vec{\tau}\psi)$, isovector-vector $(\bar{\psi}\vec{\tau}\gamma_\mu\psi) \cdot (\bar{\psi}\vec{\tau}\gamma^\mu\psi)$. A general Lagrangian can be written as a power series in the currents $\bar{\psi}\mathcal{O}_\tau\Gamma\psi$ and their derivatives, with higher-order terms representing in-medium many-body correlations.

In Ref. [33] a Lagrangian was considered that includes second-order interaction terms, with many-body correlations encoded in density-dependent strength functions. A set of 10 constants, which control the strength and density dependence of the interaction Lagrangian, was fine-tuned in a multistep parameter fit exclusively to the experimental masses of 64 axially deformed nuclei in the regions $A \approx 150$ –180 and $A \approx 230$ –250. The resulting functional DD-PC1 has been further tested in calculations of binding energies, charge radii, deformation parameters, neutron skin thickness, and excitation energies of giant monopole and dipole resonances. The corresponding nuclear matter equation of state is characterized by the following properties at the saturation point: nucleon density $\rho_{\text{sat}} = 0.152 \text{ fm}^{-3}$, volume energy $a_v = -16.06 \text{ MeV}$, surface energy $a_s = 17.498 \text{ MeV}$, symmetry energy $a_4 = 33 \text{ MeV}$, and the nuclear matter compression modulus $K_{\text{nm}} = 230 \text{ MeV}$.

For a quantitative description of open-shell nuclei it is necessary to consider also pairing correlations. The relativistic Hartree-Bogoliubov (RHB) framework [36] provides a unified description of particle-hole (ph) and particle-particle (pp) correlations on a mean-field level by combining two average potentials: the self-consistent mean field that encloses all the long range ph correlations, and a pairing field $\hat{\Delta}$ that sums up the pp-correlations. In this work we perform axially symmetric and triaxial calculations based on the RHB framework with the ph effective interaction derived from the DD-PC1 functional. A pairing force separable in momentum space: $\langle k|V^{150}|k'\rangle = -Gp(k)p(k')$ is used in the pp channel. By assuming a simple Gaussian ansatz $p(k) = e^{-a^2k^2}$, the two parameters G and a were adjusted to reproduce the density dependence of the gap at the Fermi surface in nuclear matter, calculated with a Gogny force. For the DIS parameterization [37] of the Gogny force the following values were determined: $G = -728 \text{ MeVfm}^3$ and $a = 0.644 \text{ fm}$ [38]. When transformed from momentum to coordinate space, the force takes the form

$$V(\mathbf{r}_1, \mathbf{r}_2, \mathbf{r}'_1, \mathbf{r}'_2) = G\delta(\mathbf{R} - \mathbf{R}')P(\mathbf{r})P(\mathbf{r}')\frac{1}{2}(1 - P^\sigma), \quad (1)$$

where $\mathbf{R} = \frac{1}{2}(\mathbf{r}_1 + \mathbf{r}_2)$ and $\mathbf{r} = \mathbf{r}_1 - \mathbf{r}_2$ denote the center-of-mass and the relative coordinates, and $P(\mathbf{r})$ is the Fourier transform of $p(k)$: $P(\mathbf{r}) = 1/(4\pi a^2)^{3/2}e^{-\mathbf{r}^2/4a^2}$. The pairing force has finite range and, because of the presence of the factor $\delta(\mathbf{R} - \mathbf{R}')$, it preserves translational invariance. Even though $\delta(\mathbf{R} - \mathbf{R}')$ implies that this force is not completely separable in coordinate space, the corresponding antisymmetrized pp matrix elements can be represented as a sum of a finite number of separable terms in the basis of a 3D harmonic oscillator [39]. The force Eq. (1) reproduces pairing properties of spherical and deformed nuclei calculated with the original Gogny force, but with the important advantage that the computational cost is greatly reduced.

The Dirac-Hartree-Bogoliubov equations [36] are solved by expanding the nucleon spinors in the basis of a 3D harmonic oscillator in Cartesian coordinates. In this way both axial and triaxial nuclear shapes can be described. The map of the energy surface as a function of the quadrupole deformation is obtained by imposing constraints on the axial and triaxial quadrupole moments. The method of quadratic constraint uses an unrestricted variation of the function

$$\langle \hat{H} \rangle + \sum_{\mu=0,2} C_{2\mu}(\langle \hat{Q}_{2\mu} \rangle - q_{2\mu})^2, \quad (2)$$

where $\langle \hat{H} \rangle$ is the total energy, and $\langle \hat{Q}_{2\mu} \rangle$ denotes the expectation value of the mass quadrupole operators:

$$\hat{Q}_{20} = 2z^2 - x^2 - y^2 \quad \text{and} \quad \hat{Q}_{22} = x^2 - y^2. \quad (3)$$

$q_{2\mu}$ is the constrained value of the multipole moment, and $C_{2\mu}$ is the corresponding stiffness constant.

To illustrate the accuracy of the DD-PC1 functional in the calculation of ground-state properties of heavy nuclei, in Fig. 1 we plot the results of self-consistent 3D RHB calculations for several isotopic chains in the actinide region: Th, U, Pu, Cm, Cf, Fm, and No. The deviations of the calculated binding energies from data [40] show an excellent agreement

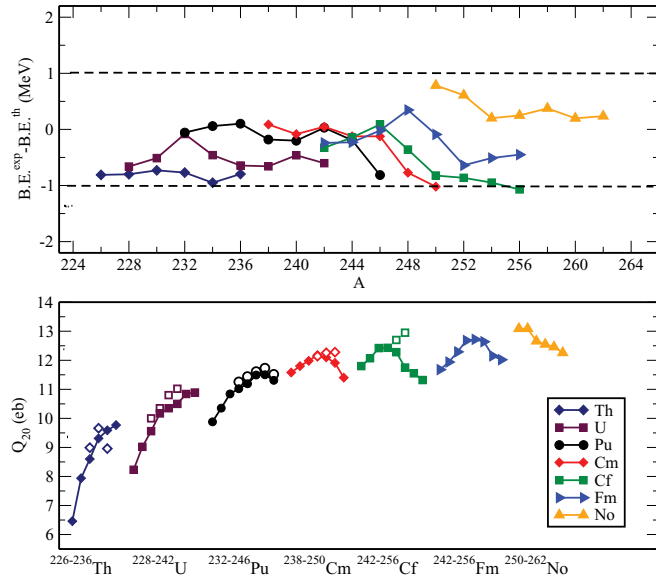


FIG. 1. (Color online) Absolute deviations of the self-consistent RHB ground-state binding energies from the experimental values [40], for the isotopic chains of Th, U, Pu, Cm, Cf, Fm, and No (upper panel). In the lower panel the calculated ground-state axial quadrupole moments are shown in comparison to data [41] (open symbols).

between theory and experiment: the absolute difference between calculated and experimental binding energies is less than 1 MeV in all cases. An important result is also that the mass residuals do not display any notable dependence on the mass (neutron) number. The calculated ground-state quadrupole moments are compared to available data [41] in the lower panel of Fig. 1. One notices that the values predicted by the DD-PC1 functional reproduce in detail the isotopic trend of the empirical moments in the Th, U, Pu, and Cm sequences and are in very good agreement with the quadrupole moments of the Cf isotopes.

The “double-humped” fission barriers of actinide nuclei provide an important test for nuclear energy density functionals. In the review of self-consistent mean-field models for nuclear structure [15], which also contains an extensive list of references to previous studies of fission barriers using mean-field-based models, Bender *et al.* compared paths in the deformation energy landscape of ^{240}Pu obtained with various Skyrme, Gogny and relativistic mean-field (RMF) interactions. In general, relaxing constraints on symmetries lowers the fission barriers. The predicted shapes are triaxial and reflection-symmetric at the first barrier, and predominantly axial and reflection-asymmetric at the second barrier. The systematics of axially symmetric fission barriers in Th, U, Pu, Cm, and Cf nuclei, as well as for superheavy elements $Z = 108$ – 120 , using several Skyrme and RMF mean-field interactions, was investigated in Ref. [42]. The fission barriers of 26 even- Z nuclei with $Z = 90$ – 102 , up to and beyond the second saddle point, were calculated in Ref. [43] with the constrained Hartree-Fock approach based on the Skyrme effective interaction SkM*. The fission barriers of ^{240}Pu beyond the second saddle point were also explored using the axially quadrupole constrained RMF model with the PK1

effective interaction [44]. In a very recent optimization of the new Skyrme density functional UNEDF1 [35], excitation energies of fission isomers in $^{236,238}\text{U}$, ^{240}Pu , and ^{242}Cm , were added to the data set used to adjust the parameters of the functional. Compared to the original functional UNEDF0 [34], the inclusion of the new data allowed an improved description of fission properties of actinide nuclei. The effect of triaxial deformation on fission barriers in the actinide region was recently also explored in a systematic calculation of Ref. [45], based on the RMF + BCS framework. The potential energy surfaces of actinide nuclei in the $(\beta_{20}, \beta_{22}, \beta_{30})$ deformation space (triaxial + octupole) were analyzed in the newest self-consistent mean-field plus BCS calculation based on relativistic energy density functionals [46]. This study has shown the importance of the simultaneous treatment of triaxial and octupole shapes along the entire fission path.

The fission barriers calculated in the present work are shown in Fig. 2, where we plot the potential energy curves of $^{236,238}\text{U}$, ^{240}Pu , and ^{242}Cm , as functions of the axial quadrupole deformation parameter β_{20} . The deformation parameters are related to the multipole moments by the relation

$$\beta_{\lambda\mu} = \frac{4\pi}{3AR^\lambda} \langle Q_{\lambda\mu} \rangle. \quad (4)$$

To be able to analyze the outer barrier heights considering reflection-asymmetric (octupole) shapes, the results displayed in this figure have been obtained in a self-consistent RMF plus BCS calculation that includes either triaxial shapes or axially symmetric but reflection-asymmetric shapes. The interaction in the particle-hole channel is determined by the relativistic functional DD-PC1, and a density-independent δ force is the effective interaction in the particle-particle channel. The pairing strength constants V_n and V_p are from Ref. [47], where they were adjusted, together with the parameters of the relativistic functional PC-F1, to ground-state observables (binding energies, charge and diffraction radii, surface thickness, and pairing gaps) of spherical nuclei, with pairing correlations treated in the BCS approximation. In many cases the functionals PC-F1 [47] and DD-PC1 predict similar results for ground-state properties (cf., for instance, Ref. [48]), and reproduce the empirical pairing gaps. Thus, we assume that, without any further adjustment, the same pairing strength parameters can be used in RMF + BCS calculations with the functional DD-PC1.

The solid (black) curves correspond to binding energies calculated with the constraint on the axial quadrupole moment, assuming axial and reflection symmetry. The absolute minima of these curves determine the energy scale (zero energy). The dot-dashed (blue) curves denote paths of minimal energy in calculations that break axial symmetry with constraints on quadrupole axial Q_{20} and triaxial Q_{22} moments. Finally, the dashed (green) curves are paths of minimal energy obtained in axially symmetric calculations that break reflection symmetry (constraints on the quadrupole moment Q_{20} and the octupole moment Q_{30}). The red squares, lines, and circles denote the experimental values for the inner barrier height, the excitation energy of the fission isomer, and the height of the outer barrier, respectively. The data are from Ref. [49].

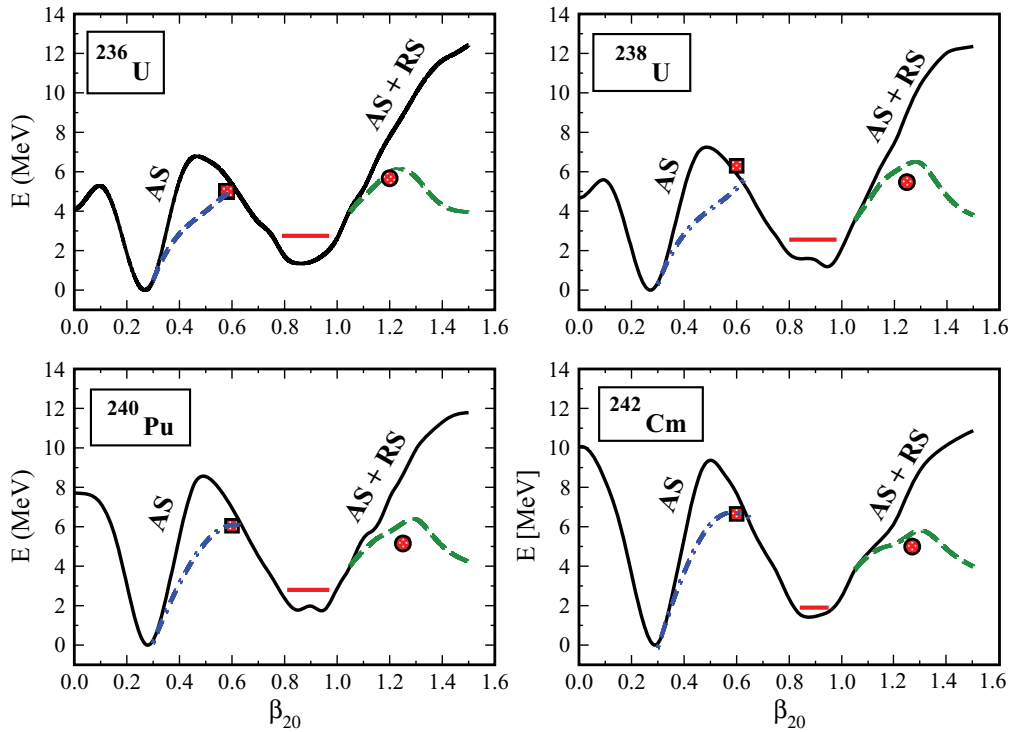


FIG. 2. (Color online) Constrained energy curves of $^{236,238}\text{U}$, ^{240}Pu , and ^{242}Cm , as functions of the axial quadrupole deformation parameter. Results of self-consistent axially and reflection-symmetric, triaxial, and axially reflection-asymmetric RMF + BCS calculations are denoted by solid (black), dot-dashed (blue), and dashed (green) curves, respectively. The red squares, lines, and circles denote the experimental values for the inner barrier height, the excitation energy of the fission isomer, and the height of the outer barrier, respectively. The data are from Ref. [49].

The excitation energies of fission isomers are fairly well reproduced by the axially symmetric and reflection symmetric calculation, but the paths constrained by these symmetries overestimate the height of the inner and outer barriers. The inclusion of triaxial shapes lowers the inner barrier by ≈ 2 MeV, that is, the axially symmetric barriers in the region $\beta_{20} \approx 0.5$ are bypassed through the triaxial region, bringing the height of the barriers much closer to the empirical values. As shown in the figure, the inclusion of octupole shapes (axial, reflection-asymmetric calculations) is essential to reproduce the height of the outer barrier in actinide nuclei. A very good agreement with data is obtained by following paths through shapes with nonvanishing octupole moments. With the present implementation of the model we could not simultaneously calculate both octupole and triaxial shapes. Such a study was recently performed in the RMF + BCS framework by Bing-Nan Lu and collaborators [46]. It was shown that not only the inner barrier, but also the reflection-asymmetric outer barrier is lowered by the inclusion of triaxial deformations. The effect on the outer barrier is of the order of 0.5–1 MeV, and it accounts for 10% to 20% of the barrier height. Considering that the functional DD-PC1 was adjusted only to the binding energies of the absolute axial minima (masses) of deformed nuclei, the results shown in Fig. 2 reproduce the experimental values surprisingly well and, therefore, appear to be very promising for its extrapolation to the region of superheavy nuclei. We note here that, except for the results of Fig. 2, all the other calculations reported in this work have been performed

in the RHB framework using the functional DD-PC1 and the separable pairing interaction Eq. (1).

Figure 3 illustrates the accuracy of the functional DD-PC1 in the axially symmetric RHB calculation of Q_α values, that is, energies of α particles emitted by even-even actinide nuclei. The calculated values are plotted in comparison to data [40].

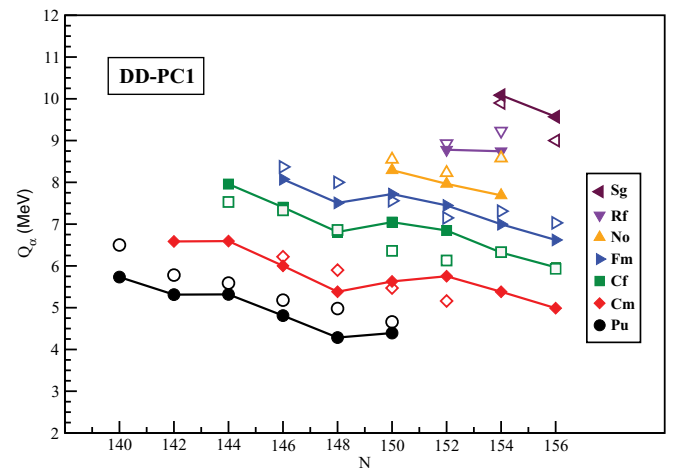


FIG. 3. (Color online) Q_α values for even-even actinide chains obtained in a self-consistent axially symmetric RHB calculations using the functional DD-PC1 and the separable pairing interaction Eq. (1). The theoretical values (filled symbols) are connected by lines and compared to data (open symbols) [40].

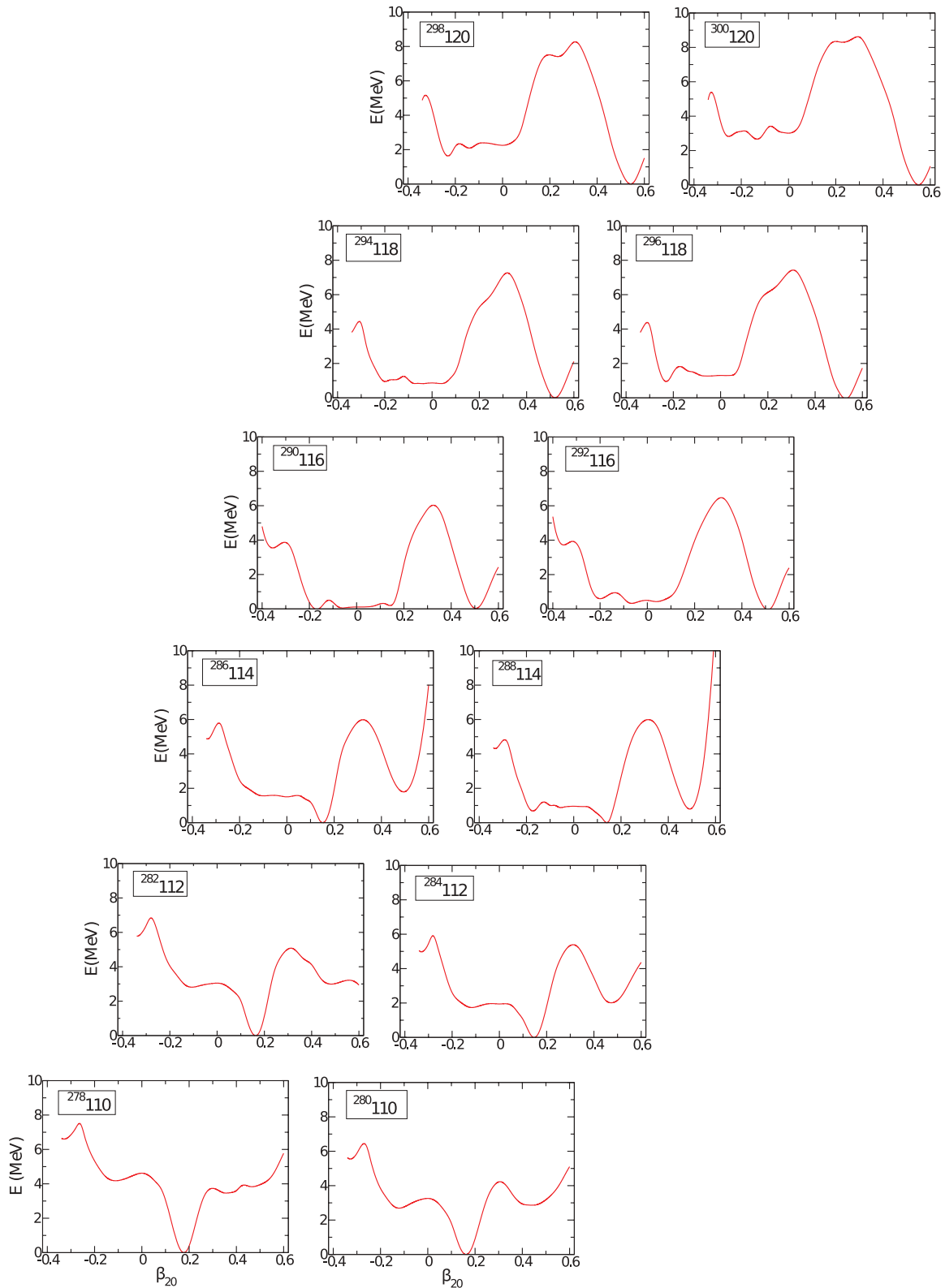


FIG. 4. (Color online) Self-consistent RHB axially symmetric energy curves of isotopes in the α -decay chains of $^{298}\text{120}$ and $^{300}\text{120}$, as functions of the quadrupole deformation parameter.

Even in this simple calculation that assumes axial symmetry, the model reproduces the empirical trend of Q_α values. The few cases for which we find a somewhat larger deviation

from data most probably point to a more complex potential energy surface, possibly including shape coexistence. It is interesting to note that on the quantitative level the theoretical

results are very similar to those obtained in the self-consistent nonrelativistic Hartree-Fock-Bogoliubov calculation based on the Skyrme functional SLy4 [13,17].

Summarizing this section, it has been shown that self-consistent mean-field calculations based on the relativistic energy density functional DD-PC1 predict binding energies, ground-state quadrupole deformations, fission barriers, fission isomers, and Q_α values for even-even actinide nuclei in very good agreement with data. In the next section we apply the RHB framework based on the functional DD-PC1 and the separable pairing interaction Eq. (1) to an illustrative study of deformed shapes and shape transitions of superheavy nuclei.

III. SHAPE TRANSITIONS IN SUPERHEAVY NUCLEI

In a very recent study of fission barriers and fission paths in even-even superheavy nuclei with $Z = 112-120$ [23],

DD-PC1 was used, together with two other relativistic energy density functionals, in a systematic RMF + BCS calculation of potential energy surfaces, including triaxial and octupole shapes. It was shown that low- Z and low- N nuclei in this region are characterized by axially symmetric inner fission barriers. With the increase of Z and/or N , in some of these nuclei several competing fission paths appear in the region of the inner barrier. Allowing for triaxial shapes lowers the outer fission barrier by 1.5–3 MeV, and in many nuclei the lowering induced by triaxiality is even more important than the one caused by octupole deformation.

The variation of ground-state shapes is governed by the evolution of shell structure of single-nucleon orbitals. In very heavy deformed nuclei, in particular, the density of single-nucleon states close to the Fermi level is rather large, and even small variations in the shell structure predicted by different effective interactions can lead to markedly distinct equilibrium deformations. To illustrate the rapid change of

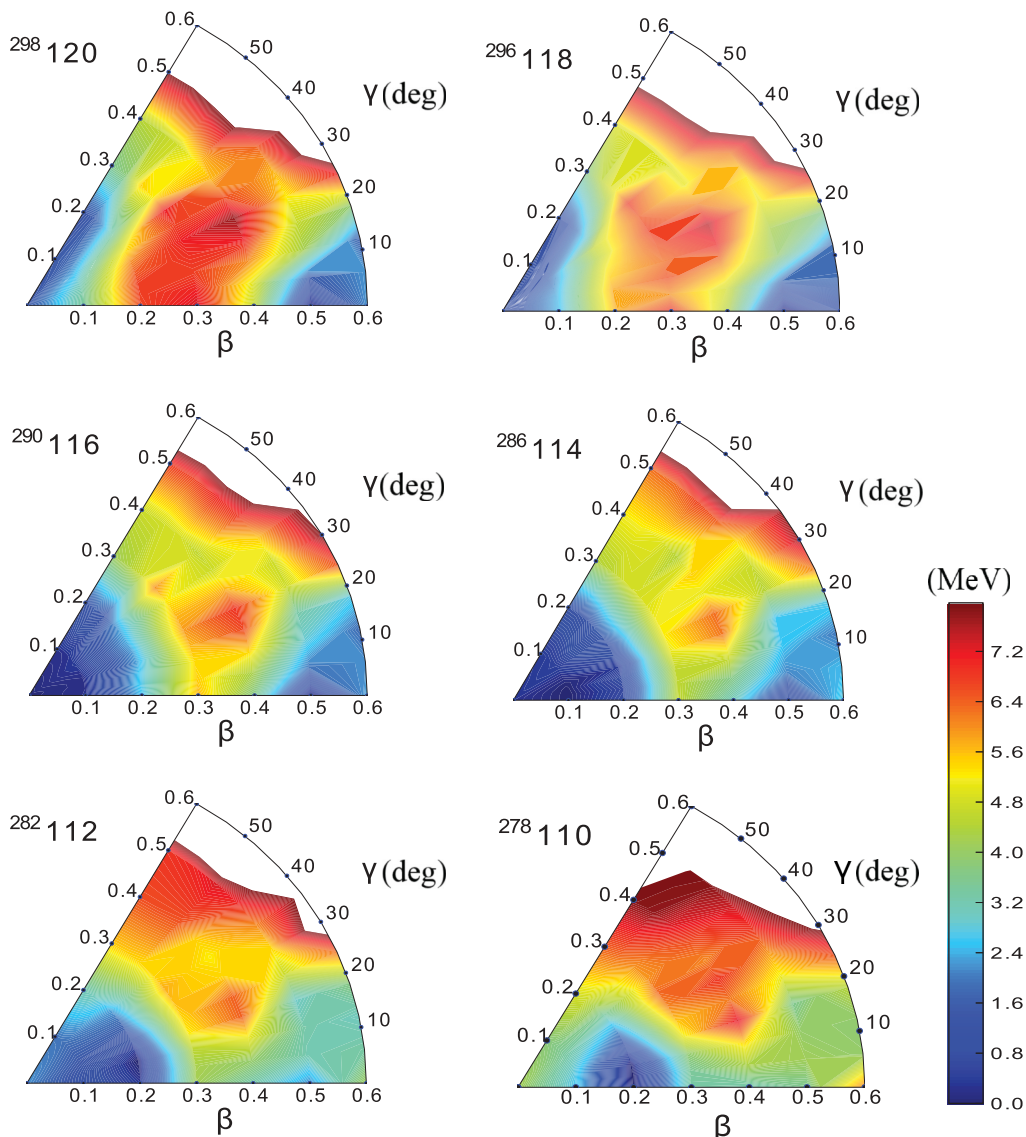


FIG. 5. (Color online) Self-consistent RHB triaxial energy maps of the even-even isotopes in the α -decay chain of $^{298}\text{120}$ in the β - γ plane ($0 \leq \gamma \leq 60^\circ$). Energies are normalized with respect to the binding energy of the absolute minimum.

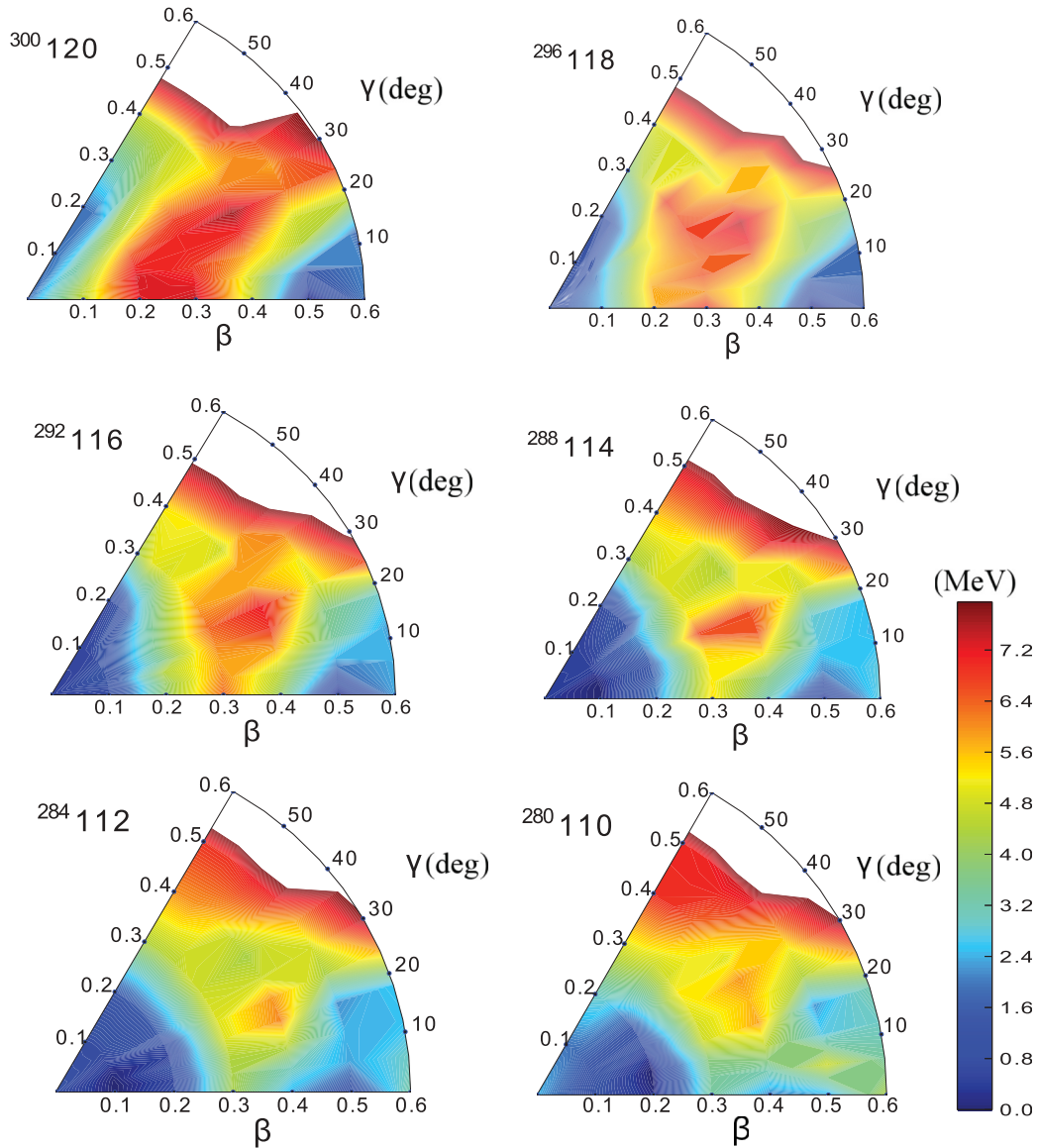


FIG. 6. (Color online) Same as described in the caption to Fig. 5 but for the the α -decay chain of $^{300}\text{120}$.

equilibrium shapes for the heaviest nuclear systems, Fig. 4 displays the results of self-consistent axially symmetric RHB calculations of isotopes in the α -decay chains of two superheavy nuclei, $^{298}\text{120}$ and $^{300}\text{120}$, respectively. The quadrupole energy curves are plotted as functions of the deformation parameter β_{20} . Lighter systems around $Z = 110$ are characterized by well-developed prolate minima around $\beta_{20} \approx 0.2$, whereas intermediate nuclei display both oblate and prolate minima at small deformation, and the heaviest isotopes appear to be slightly oblate. Another characteristic of the energy curves is the shift of the saddle point to smaller deformations with the increase in the mass number, while the barriers become wider. Since the prolate and oblate minima can be connected through triaxial shapes without a barrier, these energy curves show the importance of performing more realistic calculations, including triaxial, and for large deformations, octupole shapes.

This is shown in Figs. 5 and 6, where we plot the corresponding triaxial RHB energy surfaces in the β - γ plane ($0 \leq \gamma \leq 60^\circ$) for isotopes in the α -decay chains of $^{298}\text{120}$ and $^{300}\text{120}$, respectively. In both chains the heaviest systems display soft oblate axial shapes with minima that extend from the spherical configuration to $|\beta_{20}| \approx 0.4$ ($Z = 120$) and $|\beta_{20}| \approx 0.3$ ($Z = 118$). We do not have to consider the deep prolate minima at $\beta_{20} > 0.5$ because the inclusion of reflection asymmetric shape degrees of freedom (octupole deformation) drastically reduces or removes completely the outer barrier. A low outer barrier implies a high probability for spontaneous fission, such that the prolate superdeformed states are not stable against fission [50]. In contrast to the actinides shown in Fig. 2, superheavy nuclei are actually characterized by a “single-humped” fission barrier. As already noted, in the present implementation of the model triaxial and octupole deformations cannot be taken into account simultaneously.

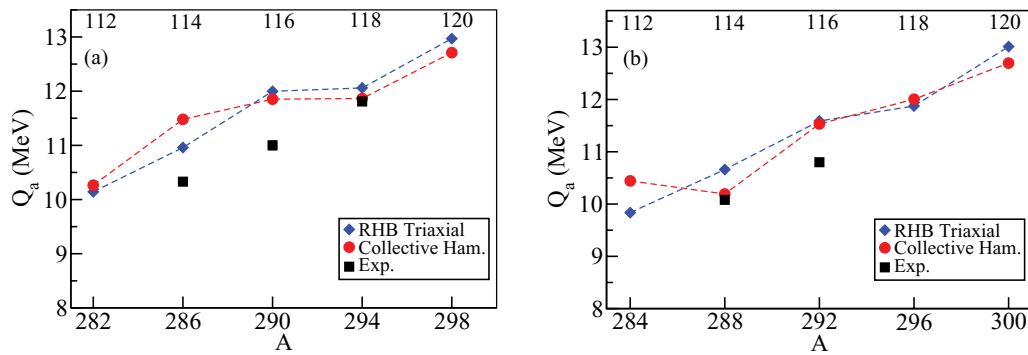


FIG. 7. (Color online) Q_α values for the α -decay chains of $^{298}120$ (a) and $^{300}120$ (b). The theoretical values are calculated as the difference between the mean-field minima of the parent and daughter nuclei (blue diamonds) and as the difference between the energies of the 0^+ ground states of the quadrupole collective Hamiltonian (red circles). The data (squares) are from Ref. [24].

Reflection asymmetric shape degrees of freedom, however, play no role at small and moderate deformations that characterize ground-state configurations of the superheavy systems considered here. The intermediate nuclei with $Z = 116$ are essentially spherical but soft both in β and γ , whereas prolate deformed mean-field minima develop in the lighter systems with $Z = 114$, $Z = 112$, and $Z = 110$. The predicted evolution of shapes is consistent with results obtained using the self-consistent Hartree-Fock-Bogoliubov framework based on Skyrme functionals [6,10,17].

The two main decay modes in this region are α emission and spontaneous fission. The theoretical α -decay energies, denoted by (blue) diamonds in Fig. 7, are calculated as the difference between the absolute minima of the energy maps of the parent and daughter nuclei, shown in Figs. 5 and 6. For the mean-field ground state we take the minimum with the highest barrier with respect to fission, that is, we do not consider superdeformed minima with very low fission barriers. The theoretical Q_α values are shown in comparison to available data for the α -decay properties of superheavy nuclei [24]. The trend of the data is obviously reproduced by the calculations, and the largest difference between theoretical and experimental values is less than 1 MeV. This is a rather good result, considering that equilibrium nuclear shapes change rapidly in

the two α -decay chains and that the calculation is performed on the mean-field level. In general, the level of agreement with experiment is similar to the one found in the case of actinide nuclei (cf. Fig. 3), but not quite the same as that obtained using the macro-micro model specially adapted to heaviest nuclei (HN) [5,51–53]. It is interesting, though, that our prediction both for the α -decay energy and half-life of the $A = 298$ isotope of the new element $Z = 120$ are consistent with those of the HN macro-micro model [53].

Alpha-decay half-lives are calculated using a simple five-parameter phenomenological Viola-Seaborg-type formula [5,54]. The parameters of this formula were adjusted to experimental half-lives and Q_α values of more than 200 nuclei with $Z = 84$ –111 and $N = 128$ –161 [54]. Using the theoretical Q_α values plotted in Fig. 7 as input, the resulting half-lives are compared to available data [24] in Fig. 8. A rather good agreement with experiment is obtained for both decay chains.

The theoretical values denoted by (blue) diamonds in Figs. 7 and 8 correspond to transitions between the self-consistent mean-field minima on the triaxial RHB energy surfaces shown in Figs. 5 and 6. Such a calculation does not explicitly take into account collective correlations related to symmetry restoration and to fluctuations in the collective

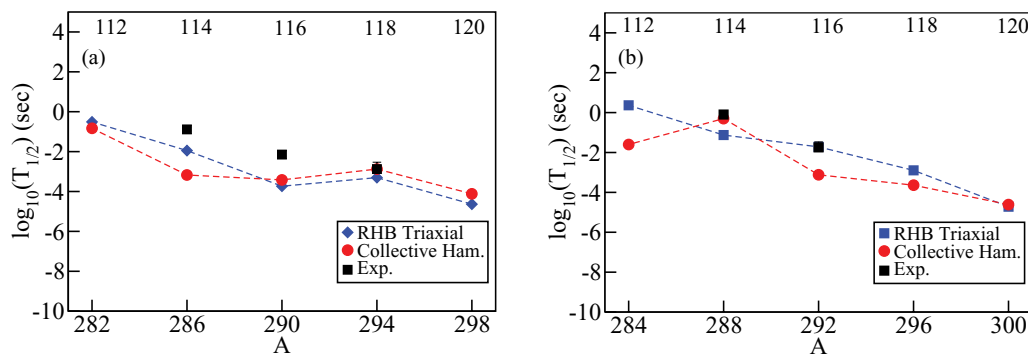


FIG. 8. (Color online) Half-lives for the α -decay chains of $^{298}120$ (a) and $^{300}120$ (b). The theoretical values are calculated from a phenomenological Viola-Seaborg-type formula [5,54], using the Q_α values from Fig. 7. Diamonds correspond to values of Q_α calculated from mean-field RHB solutions, whereas circles denote half-lives computed using Q_α values determined by the 0^+ ground states of the quadrupole collective Hamiltonian. The data (squares) are from Ref. [24].

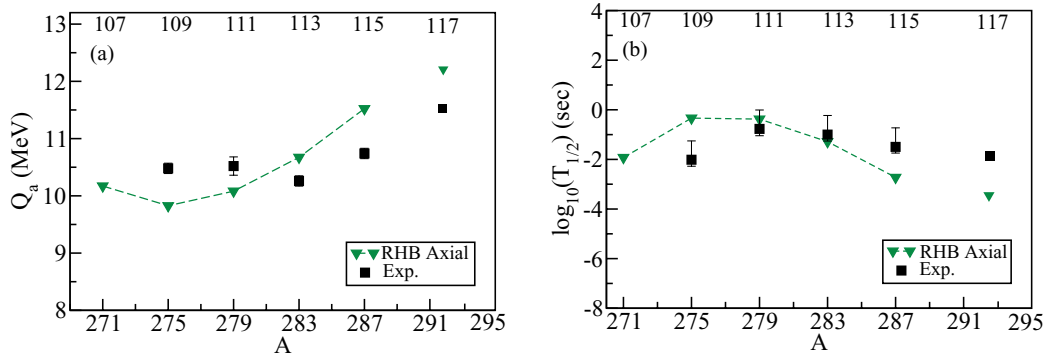


FIG. 9. (Color online) Q_α values (a) and half-lives (b) for the α -decay chain of $^{287}115$ and for the nucleus $^{293}117$.

coordinates β and γ . Physical transitions occur, of course, not between mean-field minima but between states with definite angular momentum. In cases in which both the initial and final states have similar deformation this will not make a large difference for the Q_α values, because collective correlations are implicitly taken into account in energy density functionals through the adjustment of parameters to ground-state properties (masses). The difference, however, can be larger in cases when the equilibrium shapes of the parent and daughter nucleus correspond to rather different deformations, because the collective correlation energy generally increases with deformation. For this reason we have also used a recent implementation of the collective Hamiltonian based on relativistic energy density functionals [55], to calculate α -transition energies between ground states of even-even nuclei ($0^+ \rightarrow 0^+$ transitions). Starting from self-consistent single-nucleon orbitals, the corresponding occupation probabilities and energies at each point on the energy surfaces shown in Figs. 5 and 6, the mass parameters and the moments of inertia of the collective Hamiltonian are calculated as functions of the deformations β and γ . The diagonalization of the Hamiltonian yields excitation energies and collective wave functions that can be used to calculate various observables. The (red) circles in Figs. 7 and 8 denote the Q_α values and half-lives, respectively, computed for transitions $0_{g.s.}^+ \rightarrow 0_{g.s.}^+$ between eigenstates of the collective Hamiltonian. The differences with respect to mean-field values are not large, especially for the heaviest, weakly oblate deformed or spherical systems. For the lighter

prolate and more deformed nuclei, the differences can be as large as the deviations from experimental values.

In Figs. 9 and 10 we plot the Q_α values and half-lives for a chain of odd-even and odd-odd superheavy systems, respectively, in comparison with available data [24,26]. The Q_α values are computed as energy differences between mean-field axial RHB minima of parent and daughter nuclei. The minima are determined in the blocking approximation for the odd proton (odd-even nuclei) and the odd proton and odd neutron (odd-odd nuclei). The equilibrium deformations are determined from the axial energy minima of the corresponding even-even systems, and the equilibrium odd-even (odd-odd) configuration is the one that minimizes the RHB total energy of the odd-even (odd-odd) system by blocking the odd-proton (odd-proton and odd-neutron) Nilsson orbitals. Because one needs to block several Nilsson orbitals in order to find the energy minimum, the calculation for odd-even and odd-odd superheavy nuclei is restricted to configurations with axial symmetry. Also in this case the model reproduces the mass dependence of Q_α values and half-lives, and only for the heaviest nuclei with $Z = 115$ and $Z = 117$ we find significant differences with respect to data. The half-lives are calculated with the Viola-Seaborg-type formula of Refs. [5,54], which takes into account the effect of the odd nucleons by reducing the transition energy with respect to Q_α by the average excitation energy of the daughter nucleus. This correction is necessary when considering ground-state to ground-state Q_α values, because the half-life is determined by the most

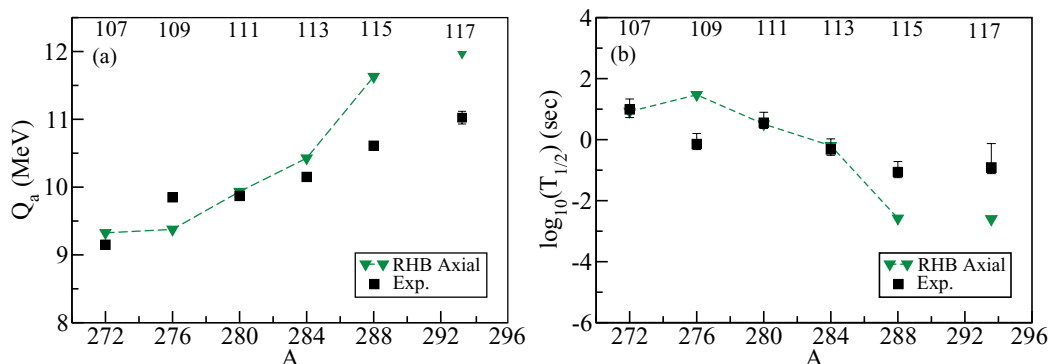


FIG. 10. (Color online) Same as described in the caption to Fig. 9 but for the α -decay chain of $^{288}115$ and for the nucleus $^{294}117$.

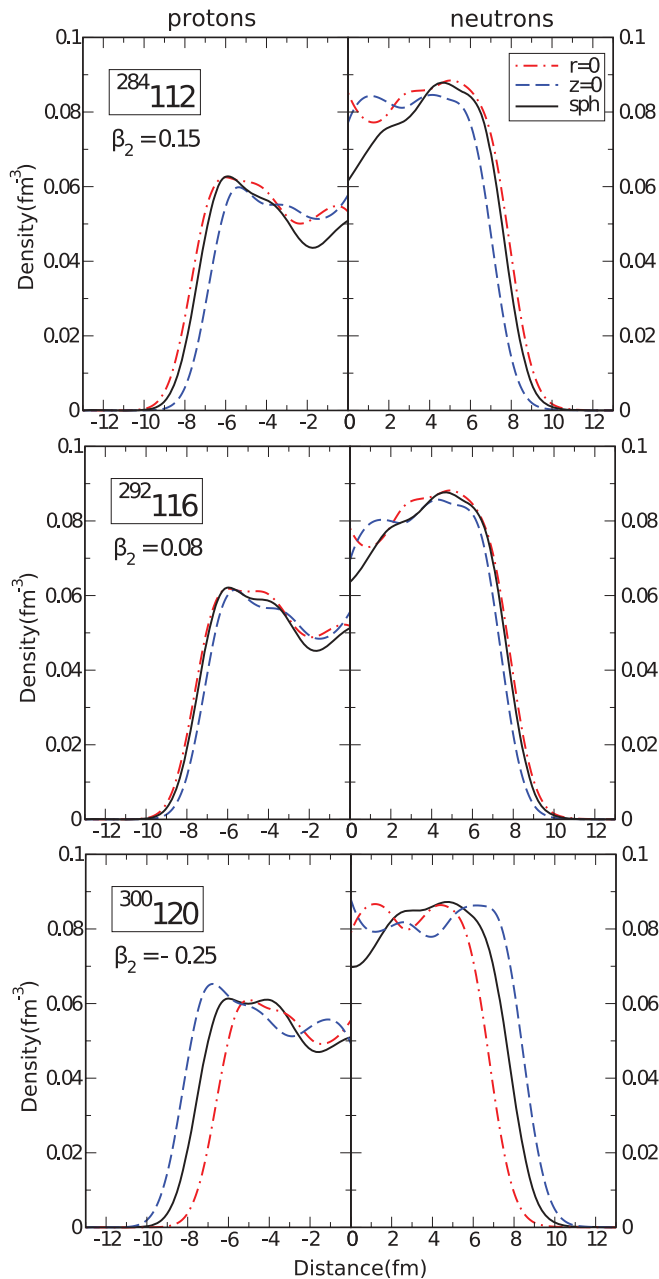


FIG. 11. (Color online) Calculated proton (left) and neutron (right) density distributions of $^{284}112$, $^{292}116$, and $^{300}120$, as functions of the distance from the center of the nucleus. The dot-dashed and dashed curves correspond to the distribution profiles $\rho(z, 0)$ along the z axis and $\rho(0, r_{\perp})$ along the r_{\perp} axis, respectively. The solid curves denote the corresponding density distributions $\rho(r)$ calculated assuming spherical shapes.

probable transition and this occurs between states with the same structure (same quantum numbers for odd-even and odd-odd nuclei). We note that a somewhat better agreement with data for $^{293}117$ and $^{294}117$ was obtained using the HN macro-micro model that includes a more realistic deformation space [52]. From the energy surfaces shown in Figs. 5 and 6, one notes that the corresponding even-even systems are soft both in β and γ and, therefore, pronounced effects of core

polarization can be expected in the odd-even and odd-odd nuclei. The detailed structure of these soft nuclei cannot, of course, be reproduced by the simple blocking approximation assuming axially symmetric shapes, as used in the present calculation. Nevertheless, the level of agreement with data on the Q_{α} values and half-lives for odd-even and odd-odd nuclei reflects the underlying structure and ordering of proton and neutron quasiparticle states predicted by the functional DD-PC1 and the separable pairing interaction.

The evolution of density distributions with proton and/or neutron number presents an interesting topic for self-consistent studies based on EDF. For superheavy nuclei, in particular, the influence of the central depression in the density distribution on the stability of spherical systems was studied [56,57]. Since high- j orbitals are localized mostly near the surface of the nucleus, whereas low- j orbitals near the center, the filling of the single-nucleon orbitals with the increase of proton and/or neutron number can affect the evolution of the radial density profile. It was shown that a large central depression leads to the spherical shell gaps at $Z = 120$ and $N = 172$, whereas a more even density profile favors $N = 184$ and leads to the appearance of a $Z = 126$ shell gap [56]. However, as it was also shown in Ref. [57], even small deformations have considerable effect of the density distributions. Similar results are also obtained in the present study. As an illustration, in Fig. 11 we plot the proton and neutron density profiles for three characteristic cases in the α -decay chain of $^{300}120$: the prolate $^{284}112$ ($\beta \approx 0.15$), the nearly spherical $^{292}116$ ($\beta \approx 0.08$), and the oblate $^{300}120$ ($\beta \approx -0.25$). The density profiles are plotted as functions of the distance from the center of the nucleus. The solid curves are obtained assuming spherical shapes and, in this case, one notices a pronounced central depression of proton and neutron densities for all three nuclei. Allowing for axial deformation can have a significant effect on the density profiles. The dot-dashed and dashed curves in Fig. 11 correspond to the distribution profiles $\rho(z, 0)$ along the z axis and $\rho(0, r_{\perp})$ along the r_{\perp} axis, respectively. In all three nuclei the central depression is reduced by deformation. The effect is not significant in the nearly spherical $^{292}116$, and in this nucleus both the proton and neutron densities display a weak central depression. The effect of deformation is much more pronounced in the prolate $^{284}112$ and oblate $^{300}120$ in which, especially for the neutrons, the spherical concavity virtually disappears. It will, of course, be interesting to study the evolution of central depressions in the density profiles of less neutron-deficient superheavy nuclei.

IV. SUMMARY AND OUTLOOK

The framework of relativistic nuclear EDFs has been applied to a study of deformation effects and shapes of superheavy nuclei. The microscopic self-consistent calculation is based on the EDF DD-PC1 [33] and a separable pairing interaction, used in the relativistic Hartree-Bogoliubov (RHB) model.

In addition to the equation of state of symmetric and asymmetric nuclear matter, the functional DD-PC1 was adjusted exclusively to the experimental masses of

64 axially deformed nuclei in the regions $A \approx 150$ – 180 and $A \approx 230$ – 250 . It is, therefore, interesting to note that, in constrained self-consistent calculations that include axially symmetric, triaxial, and reflection-asymmetric shapes, this functional reproduces not only the empirical masses, Q_α values, and equilibrium quadrupole deformations of actinide nuclei, but also the heights of the first and second fission barriers, as well as excitation energies of fission isomers. This is an important result as many modern functionals or effective interactions, used in studies of superheavy nuclei, are specifically adjusted to data on fission barriers and fission isomers.

After testing the theoretical framework in the actinide region, we have performed a self-consistent RHB calculation of triaxial shapes for two α -decay chains of superheavy nuclei, starting from $^{298}120$ and $^{300}120$. In both chains the heaviest systems display soft oblate axial shapes with minima that extend from the spherical configuration to $|\beta_{20}| \approx 0.4$ ($Z = 120$) and $|\beta_{20}| \approx 0.3$ ($Z = 118$). The intermediate nuclei with $Z = 116$ are essentially spherical but soft both in β and γ , whereas prolate deformed mean-field minima develop in the lighter systems with $Z = 114$, $Z = 112$, and $Z = 110$. The theoretical Q_α values reproduce the trend of the data, with the largest difference between theoretical and experimental values of less than 1 MeV. α -Decay half-lives are calculated using a five-parameter phenomenological Viola-Seaborg-type formula, and a good agreement with experiment is obtained for both decay chains. The Q_α values and half-lives for two chains of odd-even and odd-odd superheavy systems have been computed using a simple blocking approximation in axially symmetric self-consistent RHB calculations. The theoretical values are in rather good agreement with the experimental Q_α and half-lives, and only for the heaviest nuclei with $Z = 115$ and $Z = 117$ we find significant differences, most probably caused by the restriction to axially symmetric shapes.

For the two chains of even-even superheavy nuclei we have also explicitly considered collective correlations related to symmetry restoration and fluctuations in the quadrupole collective coordinates. These correlations are implicitly taken into account when adjusting energy density functionals to binding energies, but their explicit treatment could be important in cases when the initial and final states of an α -decay have markedly different deformations or shapes. Using a collective quadrupole Hamiltonian based on REDFs, we have calculated α -transition energies between ground states of even-even nuclei ($0^+ \rightarrow 0^+$ transitions), rather than between mean-field minima. The resulting Q_α values and half-lives do not significantly differ from the corresponding mean-field values, except for lighter prolate and more deformed nuclei, for which the differences can be as large as the deviations from experimental values.

Together with the recent RMF + BCS study of fission barriers and fission paths of Ref. [23], this work has demonstrated the potential of the new class of semiempirical REDFs for studies of shape coexistence and triaxiality in the heaviest nuclear system, including the explicit treatment of collective correlations using a microscopic collective Hamiltonian. This opens the possibility for a more detailed analysis of this region of SHN, including all presently known nuclides with $Z = 110$ – 118 , as well as spectroscopic studies of nuclei with $Z > 100$.

ACKNOWLEDGMENTS

The authors are grateful to A. V. Afanasjev, P. Möller, and P. Ring for valuable discussions, and to Bing-Nan Lu for tests and comparison of reflection-asymmetric shapes. This work was supported by the MZOS (Project No. 1191005-1010), the Croatian Science Foundation, and the Greek State Scholarships Foundation (I.K.Y.).

-
- [1] M. Brack, J. Damgaard, A. S. Jensen, H. C. Pauli, V. M. Strutinski, and C. Y. Wong, *Rev. Mod. Phys.* **44**, 320 (1972).
 - [2] P. Möller and J. R. Nix, *J. Phys. G: Nucl. Part. Phys.* **20**, 1681 (1994).
 - [3] P. Möller, J. R. Nix, W. D. Myers, and W. J. Swiatecki, *At. Data Nucl. Data Tables* **59**, 185 (1995).
 - [4] A. Sobiczewski, *Phys. Part. Nucl.* **25**, 119 (1994).
 - [5] A. Sobiczewski and K. Pomorski, *Prog. Part. Nucl. Phys.* **58**, 292 (2007).
 - [6] S. Ćwiok, J. Dobaczewski, P.-H. Heenen, P. Magierski, and W. Nazarewicz, *Nucl. Phys. A* **611**, 211 (1996).
 - [7] G. A. Lalazissis, M. M. Sharma, P. Ring, and Y. K. Gambhir, *Nucl. Phys. A* **608**, 202 (1996).
 - [8] M. Bender, K. Rutz, P.-G. Reinhard, J. A. Maruhn, and W. Greiner, *Phys. Rev. C* **58**, 2126 (1998).
 - [9] M. Bender, K. Rutz, P.-G. Reinhard, J. A. Maruhn, and W. Greiner, *Phys. Rev. C* **60**, 034304 (1999).
 - [10] S. Ćwiok, W. Nazarewicz, and P. H. Heenen, *Phys. Rev. Lett.* **83**, 1108 (1999).
 - [11] J.-F. Berger, L. Bitaud, J. Dechargé, M. Girod, and K. Dietrich, *Nucl. Phys. A* **685**, 1 (2001).
 - [12] M. Warda, J. L. Egidio, L. M. Robledo, and K. Pomorski, *Phys. Rev. C* **66**, 014310 (2002).
 - [13] P.-H. Heenen and W. Nazarewicz, *Europhys. News* **33**, 1 (2002).
 - [14] S. Goriely, M. Samyn, P.-H. Heenen, J. M. Pearson, and F. Tondeur, *Phys. Rev. C* **66**, 024326 (2002).
 - [15] M. Bender, P.-H. Heenen, and P.-G. Reinhard, *Rev. Mod. Phys.* **75**, 121 (2003).
 - [16] T. Bürvenich, M. Bender, J. A. Maruhn, and P.-G. Reinhard, *Phys. Rev. C* **69**, 014307 (2004).
 - [17] S. Ćwiok, P.-H. Heenen, and W. Nazarewicz, *Nature (London)* **433**, 705 (2005).
 - [18] J.-P. Delaroche, M. Girod, H. Goutte, and J. Libert, *Nucl. Phys. A* **771**, 103 (2006).
 - [19] J. A. Sheikh, W. Nazarewicz, and J. C. Pei, *Phys. Rev. C* **80**, 011302 (2009).
 - [20] J. Erlar, P. Klupfel, and P.-G. Reinhard, *Phys. Rev. C* **82**, 044307 (2010).
 - [21] E. V. Litvinova and A. V. Afanasjev, *Phys. Rev. C* **84**, 014305 (2011).
 - [22] Elena Litvinova, *Phys. Rev. C* **85**, 021303(R) (2012).

- [23] H. Abusara, A. V. Afanasjev, and P. Ring, *Phys. Rev. C* **85**, 024314 (2012).
- [24] Yu. Ts. Oganessian, *J. Phys. G: Nucl. Part. Phys.* **34**, R165 (2007).
- [25] S. Hofmann *et al.*, *Eur. Phys. J. A* **32**, 251 (2007).
- [26] Yu. Ts. Oganessian *et al.*, *Phys. Rev. Lett.* **104**, 142502 (2010).
- [27] Yu. Ts. Oganessian *et al.*, *Phys. Rev. C* **83**, 054315 (2011).
- [28] Yu. Ts. Oganessian *et al.*, *Phys. Rev. Lett.* **108**, 022502 (2012).
- [29] L. Stavsetra, K. E. Gregorich, J. Dvorak, P. A. Ellison, I. Dragojevic, M. A. Garcia, and H. Nitsche, *Phys. Rev. Lett.* **103**, 132502 (2009).
- [30] Ch. E. Düllmann *et al.*, *Phys. Rev. Lett.* **104**, 252701 (2010).
- [31] P. A. Ellison *et al.* *Phys. Rev. Lett.* **105**, 182701 (2010).
- [32] P. Jachimowicz, M. Kowal, and J. Skalski, *Phys. Rev. C* **83**, 054302 (2011).
- [33] T. Nikšić, D. Vretenar, and P. Ring, *Phys. Rev. C* **78**, 034318 (2008).
- [34] M. Kortelainen, T. Lesinski, J. Moré, W. Nazarewicz, J. Sarich, N. Schunck, M. V. Stoitsov, and S. Wild, *Phys. Rev. C* **82**, 024313 (2010).
- [35] M. Kortelainen, J. McDonnell, W. Nazarewicz, P.-G. Reinhard, J. Sarich, N. Schunck, M. V. Stoitsov, and S. M. Wild, *Phys. Rev. C* **85**, 024304 (2012).
- [36] D. Vretenar, A. V. Afanasjev, G. A. Lalazissis, and P. Ring, *Phys. Rep.* **409**, 101 (2005).
- [37] J. F. Berger, M. Girod, and D. Gogny, *Comp. Phys. Comm.* **63**, 365 (1991).
- [38] Y. Tian, Z. Y. Ma, and P. Ring, *Phys. Lett. B* **676**, 44 (2009).
- [39] T. Nikšić, P. Ring, D. Vretenar, Y. Tian, and Z. Y. Ma, *Phys. Rev. C* **81**, 054318 (2010).
- [40] G. Audi, A. H. Wapstra, and C. Thibault, *Nucl. Phys. A* **729**, 337 (2003).
- [41] S. Raman, C. W. Nestor, Jr., and P. Tikkanen, *At. Data Nucl. Data Tables* **78**, 1 (2001).
- [42] T. Bürvenich, M. Bender, J. A. Maruhn, and P.-G. Reinhard, *Phys. Rev. C* **69**, 014307 (2004).
- [43] L. Bonneau, P. Quentin, and D. Samsøen, *Eur. Phys. J. A* **21**, 391 (2004).
- [44] Hong-Feng Lü, Li-Sheng Geng, and Jie Meng, *Chin. Phys. Lett.* **23**, 2940 (2006).
- [45] H. Abusara, A. V. Afanasjev, and P. Ring, *Phys. Rev. C* **82**, 044303 (2010).
- [46] Bing-Nan Lu, En-Guang Zhao, and Shan-Gui Zhou, *Phys. Rev. C* **85**, 011301 (2012).
- [47] T. Bürvenich, D. G. Madland, J. A. Maruhn, and P.-G. Reinhard, *Phys. Rev. C* **65**, 044308 (2002).
- [48] Z. P. Li, T. Nikšić, D. Vretenar, P. Ring, and J. Meng, *Phys. Rev. C* **81**, 064321 (2010).
- [49] R. Capote, M. Herman, P. Obložinský, P. G. Young, S. Goriely, T. Belgia, A. V. Ignatyuk, A. J. Koning, S. Hilaire, V. A. Plujko, M. Avrigeanu, O. Bersillon, M. B. Chadwick, T. Fukahori, Zhigang Ge, Yinlu Han, S. Kailas, J. Kopecky, V. M. Maslov, G. Reffo, M. Sin, E. Sh. Soukhovitskii, and P. Talou, *Nucl. Data Sheets* **110**, 3107 (2009); Reference Input Parameter Library (RIPL-3), <http://www-nds.iaea.org/RIPL-3/>.
- [50] P. Möller, A. J. Sierk, T. Ichikawa, A. Iwamoto, R. Bengtsson, H. Uhrenholt, and S. Aberg, *Phys. Rev. C* **79**, 064304 (2009).
- [51] I. Muntian, Z. Patyk, and A. Sobczewski, *Acta Phys. Pol. B* **32**, 691 (2001).
- [52] A. Sobczewski, *Acta Phys. Pol. B* **41**, 157 (2010).
- [53] A. Sobczewski, *Acta Phys. Pol. B* **42**, 1871 (2011).
- [54] A. Parkhomenko and A. Sobczewski, *Acta Phys. Pol. B* **36**, 3095 (2005).
- [55] T. Nikšić, Z. P. Li, D. Vretenar, L. Próchniak, J. Meng, and P. Ring, *Phys. Rev. C* **79**, 034303 (2009).
- [56] A. V. Afanasjev and S. Frauendorf, *Phys. Rev. C* **71**, 024308 (2005).
- [57] J. C. Pei, F. R. Xu, and P. D. Stevenson, *Phys. Rev. C* **71**, 034302 (2005).